Journal of Computational Physics **161,** 354–375 (2000)
doi:10.1006/jcph.2000.6515, available online at http://www.idealibrary.com on IDEAL®

Numerical Simulation of the Homogeneous Equilibrium Model for Two-Phase Flows

S. Clerc

CEA-Saclay, Commissariat à l'Energie Atomique, Bat. 470, 91191 Gif-sur-Yvette, France
E-mail: Sebastien.Clerc@cea.fr

Received April 12, 1999; revised March 13, 2000

Homogeneous equilibrium two-phase flows are characterized by important variations of the local Mach number. Indeed, the sound speed can be several orders of magnitude higher in the liquid phase than in the two-phase mixture. For the simulation of such flows, a numerical method which can handle accurately any Mach number is thus necessary. In this paper, we investigate the applicability of preconditioned finite volume schemes for these problems. Specifically, we use Roe's scheme with Turkel's preconditioning, in a time-consistent formulation which allows transient computations. We introduce an original extension of Roe's scheme to fluids with arbitrary equations of state. We establish some stability results for the method. Numerical results are given for a two-phase bump channel flow in subsonic and transonic regimes. © 2000 Academic Press

Key Words: two-phase flows; finite volume schemes; low Mach number flows; preconditioning.

1. INTRODUCTION

In compressible flows, different regimes are determined by the Mach number M. When the Mach number becomes low, the compressible equations are stiff. One can thus expect a loss of accuracy or at least of efficiency when trying to solve the compressible equations in the low Mach regime. For this reason, it is often advisable to use specific models which remove the stiffness from the equations. These models are derived by expanding the equations in terms of a reference Mach number, considered as a small parameter.

Generally, the relative pressure variations in a low Mach number flow are of order $O(M^2)$, and the acoustic waves can be neglected. If the relative density variations are small, the result of the expansion is the incompressible (or, rather, constant density) model; see e.g., [15].

On the other hand, if large variations of the density are enforced by the boundary conditions, the assumption of a constant density is not valid. This situation occurs, for instance, in natural convection when the temperature discrepancy becomes large. A specific "low Mach

0021-9991/00 $35.00

number" model, obtained by filtering out the acoustic waves, can be used in this case; see [8, 19, 21]. In this model, the relative pressure variations are still of order $O(M^2)$, but the relative density variations can now be of order $O(1)$.

Finally, computing the propagation of acoustic waves in a low Mach number flow requires a model with $O(M)$ pressure variations; see [12, 18].

These approaches assume that the Mach number is uniformly low in time and space. There are however situations when the Mach number is low only in a limited region of the space-time domain. The initial and/or boundary conditions can lead to large variations of the Mach number: consider for instance the case of a supersonic jet in a fluid at rest. The geometry can also be responsible for variations of the Mach number, as in a nozzle with a large variation of the section. Finally, variations of the Mach number can be caused by the underlying physics: acceleration of a flame and phase change phenomena. In these cases, it is impossible to define a reference Mach number and thus to expand the equations with respect to this value: compressible equations, no matter how stiff, must be used.

Most numerical methods designed for compressible flows are unable to deal with the stiffness of the equations in the low Mach regime. Indeed, although the formal order of accuracy is not changed, the magnitude of the approximation error grows linearly with $1/M$. Roughly speaking, the numerical solutions on reasonable meshes become meaningless as soon as $M < 0.1$. This phenomenon was recognized by Volpe [34] among others, analyzed heuristically by Turkel [29], and more rigorously by Guillard and Viozat [10] on regular meshes.

However, preconditioned compressible (PC) solvers [3, 5, 10, 29, 30] are able to deal with the stiffness of the equations in the low Mach regime. Comparisons with incompressible and low Mach solvers [20, 33] show the excellent quality of the numerical results for flows with a uniformly low Mach number. In other words, when a specific incompressible or low Mach model can be used, a comparable solution can be found with a PC solver. The choice between the first and the second group of methods is therefore a matter of taste: incompressible and low Mach solvers should naturally be more efficient in terms of computational time, but finite volume PC solvers have interesting properties: exact conservation, equal space interpolation, absence of a user-defined parameter, and unstructured grid capability.

Still, the real advantage of the preconditioned compressible solvers is their ability to simulate flows that do not meet the uniform low Mach number assumption. The main purpose of the present paper is to demonstrate this ability, in the context of equilibrium two-phase flows.

Historically, the first PC solvers developed by Turkel [28] were restricted to steady-state computations. This fact has somewhat limited the interest of the CFD community in these solvers. It thus seems important to note that time-accurate PC solvers do exist and are able to simulate accurately unsteady flows. Explicit PC solvers can be made time-accurate by using a dual time-stepping algorithm (see [2, 31]), but the most natural and efficient way to restore time-accuracy is to use implicit time-stepping; see [10, 5]. We will develop this point and illustrate it by numerical examples.

In the time-consistent approach, preconditioning only affects the artificial viscosity matrix of upwind schemes. In this paper, we will study the sub-class of preconditioners which can be symmetrized along with the quasi-linear equations. For this class of preconditioners, we show that the preconditioned viscosity matrix of the upwind scheme is a well-defined positive semi-definite matrix. As a corollary, we prove that the implicit scheme is linearly stable on arbitrary grids.

Recently, Bijl and Wesseling [1] introduced a pressure-based numerical method on staggered grids which can be used for variable Mach number flows. This method seems to be a promising alternative to PC solvers. The use of staggered grids and the correction step makes the implementation somewhat more difficult than upwind PC solvers. On the other hand, the pressure correction scheme becomes an incompressible solver when $M = 0$, which is not the case with the PC approach.

Let us now briefly give the outline of the paper. In Section 2, we present the homogeneous equilibrium two-phase flow model, with a particular emphasis on the variations of the sound speed.

In Section 3, we introduce the time-consistent PC finite volume scheme and we establish some properties of the scheme. Our preconditioned numerical flux is based on Roe's scheme. We detail our extension of Roe's scheme for the equilibrium equation of state. Details on the preconditioning strategy are given in Section 4.

Section 5 deals with numerical results. To illustrate the improvement brought about by the preconditioner, we compute the evolution of a point-wise disturbance in a subsonic uniform flow. Then, we compute an equilibrium two-phase flow in a simple "bump channel" geometry. We present steady-state subsonic and transonic solutions and an unsteady computation with variable boundary conditions.

Finally, we draw some conclusions and comments in Section 6.

2. THE HOMOGENEOUS EQUILIBRIUM MODEL FOR TWO-PHASE FLOWS

2.1. *Introduction*

In this section, we briefly introduce the homogeneous equilibrium model (HEM) for two-phase flows. For further details, we refer the interested reader to the classical articles of Stewart and Wendroff [26, Sect. 4.3] and Menikoff and Plohr [16, Sect. V]. In spite of its simplicity, this model has often been used for the simulation of heat exchangers (see, e.g., [9, 22, 27]) and for the analysis of critical two-phase flows in variable section ducts (see [24] and the references therein). It is particularly well-adapted to the simulation of dispersed bubbly flow.

The shortcomings of this model are well known: it cannot reproduce strong kinetic or thermodynamic non-equilibrium effects such as occur, for instance, in annular flows or gas flows with droplets. When non-equilibrium effects are small, they can be accounted for by correction terms (drift flux velocity, subcooled boiling models). When they are more important, additional equations are needed for an accurate prediction. To account for kinetic non-equilibrium effects, one has to introduce a balance equation for the momentum of each phase. This leads to the so-called two-fluid models, which are more complex to analyze and simulate than the HEM. Thermodynamic non-equilibrium, on the other hand, is relatively easier to handle, since it does not affect directly the dynamics of the flow. A balance equation for the mass of one of the phase can be added to the mixture mass conservation equation, with appropriate mass transfer source terms for phase change.

This work however is restricted to the homogeneous equilibrium model. Our reason for choosing this simpler model is to underline one specific aspect of two-phase flows, namely the large variations of the sound speed. This feature exists in other more sophisticated models, in which additional modeling and numerical problems arise. Much effort has been spent so far on the simulation of flows in which both phases are always present, albeit at very small concentrations. Paradoxically, it turns out that the transition between pure

liquid and two-phase flows is more difficult to compute, because of the brutal change of compressibility.

A different and perhaps more difficult problem occurs at the transition between pure vapor and two-phase mixture: the equation of state exhibits a non-convex behavior which can yield non-unique solutions (see [13, 16]). In this case, the use of the HEM is therefore questionable. This phenomenon is however outside the scope of this paper.

2.2. *Equations*

In the homogeneous equilibrium model of liquid/vapor flows, we assume that the phases are in kinematic and thermodynamic equilibrium. The phases share the same pressure, temperature, and velocity. Therefore, the evolution of the mixture can be described by Euler equations for a single fluid

$$\partial_t \rho + \operatorname{div}(\rho \mathbf{u}) = 0, \tag{1}$$

$$\partial_t \rho \mathbf{u} + \operatorname{div}(\rho \mathbf{u} \otimes \mathbf{u}) + \nabla p = 0, \tag{2}$$

$$\partial_t \rho E + \operatorname{div}(\rho \mathbf{u} H) = 0. \tag{3}$$

Here $E = e + |\mathbf{u}|^2/2$ denotes the total energy and $H = h + |\mathbf{u}|^2/2$ the total enthalpy of the mixture. To close the system, the equation of state links the pressure p to the conservative thermodynamic variables ρ and ρe. The pressure law must be such that the partial derivatives χ and κ with respect to ρ and ρe satisfy

$$\kappa h + \chi > 0.$$

The sound speed c of the fluid is the square root of this quantity.

2.3. *Equation of State*

The equilibrium equation of state is more conveniently expressed as a function which gives the density of the mixture ρ in terms of the pressure p and the enthalpy of the mixture h. Suppose we know the density of each phase as a function of the pressure p and enthalpy h: $\rho_\ell(p, h)$ for the liquid and $\rho_v(p, h)$ for the vapor. Moreover, the values of the enthalpy of each phase at saturation are given as functions of the pressure: $h_\ell^{\text{sat}}(p)$ for the liquid, $h_v^{\text{sat}}(p)$ for the vapor. We first define the quality x of the mixture as

$$x = \frac{h - h_\ell^{\text{sat}}}{h_v^{\text{sat}} - h_\ell^{\text{sat}}}.$$

If $x < 0$, then the density of the fluid is that of the liquid, $\rho = \rho_\ell(p, h)$. Similarly, if $x > 1$, then the density is that of the vapor, $\rho = \rho_v(p, h)$. In the two-phase domain, i.e., when $0 \le x \le 1$, the density is given by

$$\frac{1}{\rho} = x \frac{1}{\rho_v^{\text{sat}}} + (1 - x) \frac{1}{\rho_\ell^{\text{sat}}},$$

where the density at saturation of phase k satisfies, for continuity,

$$\rho_k^{\text{sat}}(p) = \rho_k\big(p, h_k^{\text{sat}}(p)\big).$$

In practice, the functions $\rho_k(p, h)$ and $h_k^{\text{sat}}(p)$ are given as bi-cubic and cubic splines with tabulated values. The partial derivatives of the equation of state can be computed by

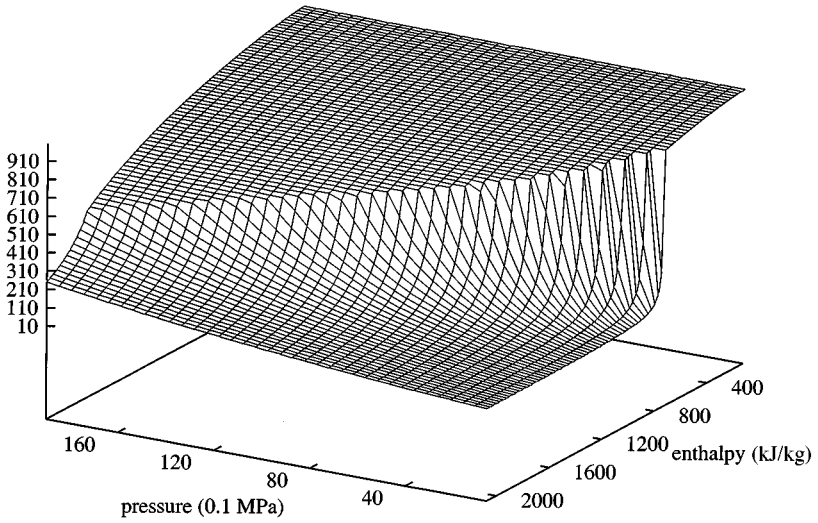

FIG. 1. Equilibrium equation of state for water, ρ as a function of p and h. The derivatives of the equation are discontinuous along the saturation line which separates the liquid (rear) from the two-phase domain (front). The discontinuity is stronger for lower values of the pressure.

differentiating the local interpolation function. In the framework of the conservative Euler equations, it is useful to express p as a function of the thermodynamic conservative variables ρ and ρe: this can be done using Newton's method.

The main characteristic of the equilibrium equation of state is the presence of a "kink" (discontinuity in the derivatives) along the saturation curve which separates the single phase and the two-phase domains. This fact is clearly visible in Fig. 1, which shows the equilibrium equation of state for water. This kink is responsible for the large variation of the sound speed. For instance, the sound speed in the liquid at saturation under a pressure of 5 Mpa is 1080 $\mathrm{m} \cdot \mathrm{s}^{-1}$, and 34 $\mathrm{m} \cdot \mathrm{s}^{-1}$ in the mixture.

3. FINITE VOLUME SCHEME AND NUMERICAL FLUX

3.1. *Finite Volume Discretization*

The Euler equations take the form of a system of conservation laws,

$$\partial_t U + \operatorname{div} \mathbf{F}(U) = 0. \tag{4}$$

We want to discretize this system by a finite volume method. Let us consider a triangulation of the computational domain by polygonal cells. For a cell K, we denote by $|K|$ its volume, ∂K its boundary, and $\mathcal{N}(K)$ the set of neighboring cells. If $J \in \mathcal{N}(K)$, the common interface is thus $\partial K \cap \partial J$: its surface is $|\partial K \cap \partial J|$ and $\mathbf{n}_{KJ}$ denotes the unit normal to the interface, oriented from K to J. Finally, we denote by δt the step of the time discretization.

The finite volume method for the solution of the system of conservation laws (4) takes the form

$$\frac{|K|}{\delta t}\left(U_K^{n+1} - U_K^n\right) + \sum_{J \in \mathcal{N}(K)} |\partial K \cap \partial J| \Phi_{KJ} = 0. \tag{5}$$

Here, U_K^n denotes the average value of the solution in the cell K, at time $n\delta t$.

To completely determine the numerical method, we have to specify the expression of the numerical flux Φ_{KJ} in terms of the cell average values. As usual, first order schemes are obtained if Φ_{KJ} depends on the two neighboring cell values U_K and U_J: $\Phi_{KJ} = \Phi(\mathbf{n}_{KJ}, U_K, U_J)$. Higher order schemes can be constructed on this basis if U_K and U_J are replaced by appropriate interpolations.

Finally, the cell values can be taken either at time $n\delta t$ (explicit time-stepping) or $(n+1)\delta t$ (implicit time-stepping). In the latter case, an approximate or exact Jacobian of the numerical flux is needed. This point is addressed in more detail in [6].

3.2. *Roe's Scheme*

The starting point of our numerical scheme is Roe's flux [23],

$$\Phi(\mathbf{n}, U_L, U_R) = \frac{1}{2}(\mathbf{F}(U_L) + \mathbf{F}(U_R)) \cdot \mathbf{n} - \frac{1}{2}|\mathbf{A}_\mathbf{n}|(U_R - U_L). \tag{6}$$

Here $\mathbf{A}_\mathbf{n} = \mathbf{A}_\mathbf{n}(U_L, U_R)$ is the so-called Roe matrix for the system. From now on, we will drop the subscript $\mathbf{n}$ for brevity, whenever possible. The numerical viscosity matrix is defined by $|\mathbf{A}| = \sum_i |\lambda_i| \mathbf{r}_i \otimes \mathbf{l}_i$, if $\mathbf{A} = \sum_i \lambda_i \mathbf{r}_i \otimes \mathbf{l}_i$ is the eigen-decomposition of $\mathbf{A}$.

For completeness, we give a compact and efficient algorithm to compute Roe's numerical flux. We first introduce average values for the density, velocity, total enthalpy, and speed of sound. For the first three, we use Roe's definition,

$$\tilde{\rho} = \sqrt{\rho_L \rho_R}, \qquad \tilde{\mathbf{u}} = \frac{\sqrt{\rho_L}\mathbf{u}_L + \sqrt{\rho_R}\mathbf{u}_R}{\sqrt{\rho_L} + \sqrt{\rho_R}}, \qquad \tilde{H} = \frac{\sqrt{\rho_L}H_L + \sqrt{\rho_R}H_R}{\sqrt{\rho_L} + \sqrt{\rho_R}}. \tag{7}$$

The average value for the speed of sound c will be discussed later. Finally, let $\tilde{u}_n = \tilde{\mathbf{u}} \cdot \mathbf{n}$ be the normal component of the velocity. The numerical flux is computed with the following algorithm:

DEFINITION 3.1 (Algorithm 1).

- If $|\tilde{u}_n| > c$, the scheme is totally upwind:
  —if $\tilde{u}_n > 0$, $\Phi = F(U_L)$,
  —if $\tilde{u}_n < 0$, $\Phi = F(U_R)$.
- In the subsonic case $|\tilde{u}_n| \le c$:
  —if $\tilde{u}_n > 0$, $\Phi = F(U_L) + (\tilde{u}_n - c)(\Delta U)^-$
  —if $\tilde{u}_n \le 0$, $\Phi = F(U_R) - (\tilde{u}_n + c)(\Delta U)^+$.

It remains to give the definition for $(\Delta U)^\pm$,

$$(\Delta U)^\pm = \frac{[\![p]\!] \pm \tilde{\rho} c [\![u_n]\!]}{2c^2} \begin{pmatrix} 1 \\ \tilde{\mathbf{u}} \pm c\mathbf{n} \\ \tilde{H} \pm \tilde{u}_n c \end{pmatrix},$$

where the notation $[\![\alpha]\!]$ stands for the jump between the left and right values of the quantity α, i.e., $\alpha_R - \alpha_L$.

3.3. *Choice of the Average Sound Velocity*

In the case of a perfect gas, Roe suggested the following average value for c,

$$c^2 = (\gamma - 1)[\tilde{H} - \tilde{\mathbf{u}} \cdot \tilde{\mathbf{u}}/2].$$

This choice leads to the following property:

PROPERTY 3.1. *If* $F(U_L) = F(U_R)$, then $\Phi = F(U_L) = F(U_R)$.

An immediate corollary of this property is the fact that stationary shocks (even non-entropic ones) are preserved by Roe's flux. For the proof of these statements, we refer to [23].

This property was extended to general equations of state by [32], among others. Their choice for the average sound of speed is

$$c^2 = \bar{\kappa}[\tilde{H} - \tilde{\mathbf{u}} \cdot \tilde{\mathbf{u}}/2] + \bar{\chi},$$

where $\bar{\kappa}$ and $\bar{\chi}$ are averaged values for the partial derivatives of the pressure, satisfying

$$[\![p]\!] = \bar{\kappa}[\![\rho e]\!] + \bar{\chi}[\![\rho]\!].$$

In this context, several authors have proposed different ways to construct the average values $\bar{\kappa}$ and $\bar{\chi}$; see for instance [17, 27, 32]. Unfortunately, no decisive physical or numerical argument can be advanced in favor of any of these methods.

Another problem is posed by the presence of discontinuous pressure derivatives in the HEM. Indeed, any attempt to compute average values of discontinuous quantities becomes hazardous. Specifically, the average values could yield a non-positive value for c^2, which would doom the numerical flux.

Instead we propose to use the algorithm of Definition 3.1 and define the average value c directly without using $\bar{\kappa}$ and $\bar{\chi}$. Such choices generally do not satisfy Property 3.1. This property is generally thought to be a crucial aspect of Roe's numerical flux. However, our experience shows that infringing upon this property by choosing other definitions for c can improve the robustness and the simplicity of the scheme without serious impact on the precision. This aspect will be the subject of a coming paper. In the present work, our main interest is in avoiding the determination of the average coefficients $\bar{\kappa}$ and $\bar{\chi}$.

If the left and right states are both in the liquid or in the mixture domain, we use the average value

$$c = \max(c_L, c_R).$$

If not, we use the choice

$$c = \min(c_L, c_R).$$

Experience shows that this choice leads to a robust and efficient scheme in subsonic and transonic regimes.

4. PRECONDITIONING FOR LOW MACH NUMBER FLOWS

4.1. *Time-Consistent vs Pseudo-Transient Preconditioning*

At this point, one can introduce two modifications in the context of low Mach number flows.

First, one can replace the time integration (5) by a preconditioned formulation,

$$\frac{|K|}{\delta t}\mathbf{P}^{-1}\left(U_K^{n+1} - U_K^n\right) + \sum_{J\in\mathcal{N}(K)} |\partial K \cap \partial J|\Phi_{KJ} = 0, \tag{8}$$

where $\mathbf{P}$ is a properly chosen non-singular matrix. This matrix may, or may not, depend on the local value in the cell U_K. It is clear that formulation (8) is not time-consistent. It can thus be used only for steady-state computations, to improve either the convergence of explicit schemes, or the conditioning of the Jacobian in implicit schemes.

On the other hand, the numerical flux itself can be preconditioned, replacing (6) by

$$\Phi_P(\mathbf{n}, U_L, U_R) = \frac{1}{2}(\mathbf{F}(U_L) + \mathbf{F}(U_R))\cdot\mathbf{n} - \frac{1}{2}\mathbf{P}^{-1}|\mathbf{P}\mathbf{A}_\mathbf{n}|\,(U_R - U_L)\,. \tag{9}$$

Here the preconditioner $\mathbf{P}$ may depend on U_R and U_L, or rather on an average value. This formulation is meant to improve the spatial discretization of the numerical method. Numerical examples of this improvement can be found in [5, 10, 30].

The preconditioned flux (9) can be used either in the original (5) or preconditioned (8) formulation. In the latter case, two different preconditioners may be used. As in [10], we advocate the use of the original time-consistent formulation (5), with the modified numerical flux (9). This will enable us to simulate unsteady flows (see Section 5).

We can write this implicit scheme with the usual "delta" form. Let $\delta U_K = U_K^{n+1} - U_K^n$ be the time increment of U_K. We have to solve

$$\begin{aligned}\frac{|K|}{\delta t}\delta U_K + \sum_{J\in\mathcal{N}(K)} |\partial K \cap \partial J|\left(\partial_{U_L}\Phi_P\cdot\delta U_K + \partial_{U_R}\Phi_P\cdot\delta U_J\right)\\ = \sum_{J\in\mathcal{N}(K)} |\partial K \cap \partial J|\Phi_P\left(U_K^n, U_L^n\right).\end{aligned} \tag{10}$$

Equation (10) gives the time increment δU as the result of a sparse, non-symmetric linear system. This increment is used to update the solution. We followed the common practice with Roe-type schemes of replacing the partial derivatives of the numerical flux $\partial_{U_L}\Phi_P$ and $\partial_{U_R}\Phi_P$ by simpler approximations.

More details on the implicit formulation can be found in [6].

4.2. *Choice of the Preconditioner*

Equation (9) defines a new family of fluxes, depending on the choice of the preconditioner $\mathbf{P}$. Note that if $\mathbf{P}$ is a scalar matrix, we recover the original flux (6). If not, $\mathbf{A}_\mathbf{n}$ and $\mathbf{P}$ do not commute, for almost every spatial direction $\mathbf{n}$. Thus, the viscosity matrix of the preconditioned scheme is modified: $\mathbf{P}^{-1}|\mathbf{P}\mathbf{A}_\mathbf{n}| \neq |\mathbf{A}_\mathbf{n}|$.

It is worthwhile noting that the preconditioned numerical flux does not belong to the family of approximate Riemann solvers, in the sense that it does not approximate Godunov's

flux up to second order in $\|U_R - U_L\|$. In other words, it is not linearly equivalent to Godunov's flux. The one-dimensional Riemann problem has often been regarded as an essential building block of finite volume schemes. Recently however, new fluxes were introduced, which are based on different ideas: cf. the AUSM [14] or the CUSP [11] schemes for instance.

In the 1-D case, the Riemann problem is a very relevant building block: as expected, the approximate Riemann solvers give very good results, even at low Mach number. This is not the case however for subsonic flows in higher dimensions. The reason is that shear waves in higher dimensions are incorrectly analyzed as a sum of a shear wave and an acoustic wave by the approximate Riemann solvers. The effect of these spurious acoustic waves is dramatic at low Mach number. Typically, they result in pressure and Mach number discontinuities aligned with the grid lines on a regular mesh. This phenomenon will be illustrated by a numerical example in Section 5.

Looking at the orders of magnitude of the coefficients in the Jacobian matrix **A**, Turkel [28] was able to derive a heuristic condition on the coefficients of the viscosity matrix to make the scheme accurate at low Mach numbers. According to Turkel, the viscosity matrix, expressed in primitive variables $(p, \mathbf{u}, S)$, should have the following orders of magnitude,

$$\begin{pmatrix} O(1/M^2) & O(1/M^2) & 0 \\ O(1) & O(1) & 0 \\ 0 & 0 & O(1) \end{pmatrix}.$$

As a result, the trace of the viscosity matrix should be of order $O(1/M^2)$. Since we expect this matrix to have non-negative real eigenvalues, it means that its spectral radius is also of order $O(1/M^2)$. A tedious computation shows that this is indeed true for Turkel's diagonal preconditioner and for the van Leer–Lee–Roe preconditioner; see [4, Chap. 4]. Thus, the maximum explicit time-step should be of order $O(M^2)$, instead of the expected $O(M)$ given by the CFL condition. In other words, no explicit scheme, stable under the CFL condition, can give correct results at low Mach numbers. This is consistent with the fact that time-accurate incompressible solvers always involve an implicit step, since the projection operator on the space of divergence-free vectors involves an elliptic problem.

The time-accurate preconditioned solver (5)–(9) must therefore be used with an implicit time-stepping in the low Mach number regime. To enhance the efficiency of the solver, one could think of using a semi-implicit discretization, leaving the treatment of convective waves explicit. Also, the discretization could be switched to a purely explicit one when the Mach number goes to one. As far as we know, these possibilities have not yet been explored in the framework of PC solvers.

4.3. *Symmetric Preconditioning*

In this section, we restrict ourselves to symmetrizable systems of hyperbolic equations. This framework is well suited for the study of hyperbolic systems in $\mathbb{R}^d$, $d > 1$. As is well known, this is not a serious restriction since all systems endowed with a mathematical entropy are symmetrizable (see, e.g., [25]).

We assume that the Roe matrix **A** satisfies the following property: there exists a symmetric positive definite matrix **S** such that $\mathbf{SA_n}$ is symmetric for all **n**. This property automatically implies that **A** has a complete set of real eigenvalues and eigenvectors. The usual Roe matrix for the Euler equations satisfies this property (see below).

We will require that the preconditioner $\mathbf{P}$ is such that $\mathbf{SP}$ is also symmetric positive definite. Although this property might not be valid for all existing preconditioners, it is true for two important examples: Turkel's diagonal preconditioner and the van Leer–Lee–Roe preconditioner for the Euler equations.

The following lemma proves that the viscosity matrix of the preconditioned scheme $\mathbf{P}^{-1}|\mathbf{PA}|$ (see Subsection 3.2) is well defined:

LEMMA 4.1. $\mathbf{PA}$ *has a complete set of real eigenvalues and eigenvectors.*

Proof. Let $\mathbf{R}$ be a non-singular matrix such that $\mathbf{R}^T\mathbf{R} = \mathbf{S}$. We then set $\tilde{\mathbf{A}} = \mathbf{RAR}^{-1}$ and $\tilde{\mathbf{P}} = \mathbf{RPR}^{-1}$. Since $\tilde{\mathbf{A}} = \mathbf{R}^{-T}(\mathbf{SA})\mathbf{R}^{-1}$, $\tilde{\mathbf{A}}$ is symmetric. Similarly, $\tilde{\mathbf{P}}$ is symmetric positive definite. Since $\mathbf{PA} = \mathbf{R}\tilde{\mathbf{P}}\tilde{\mathbf{A}}\mathbf{R}^{-1}$, it is sufficient to show that $\tilde{\mathbf{P}}\tilde{\mathbf{A}}$ has a complete set of real eigenvectors.

Next, let $\mathbf{Q}$ be a non-singular matrix such that $\mathbf{Q}^T\mathbf{Q} = \tilde{\mathbf{P}}$. We have

$$\tilde{\mathbf{P}}\tilde{\mathbf{A}} = \mathbf{Q}^T(\mathbf{Q}\tilde{\mathbf{A}}\mathbf{Q}^T)\mathbf{Q}^{-T}.$$

Thus, $\tilde{\mathbf{P}}\tilde{\mathbf{A}}$ is similar to a symmetric matrix, and thus has a complete set of real eigenvectors. ■

Finally, we show that the viscosity matrix $\mathbf{\Theta} = \mathbf{P}^{-1}|\mathbf{PA}|$ will indeed lead to a dissipative numerical scheme:

PROPERTY 4.1. $\mathbf{S\Theta}$ *is symmetric positive semi-definite.*

Proof. Since we have $\mathbf{S\Theta} = \mathbf{R}^T\tilde{\mathbf{\Theta}}\mathbf{R}$ with $\tilde{\mathbf{\Theta}} = \tilde{\mathbf{P}}^{-1}|\tilde{\mathbf{P}}\tilde{\mathbf{A}}|$, it suffices to show that $\tilde{\mathbf{\Theta}}$ is also symmetric positive semi-definite. An easy computation yields

$$\tilde{\mathbf{\Theta}} = \mathbf{Q}^{-1}|\mathbf{Q}\tilde{\mathbf{A}}\mathbf{Q}^T|\mathbf{Q}^{-T},$$

which makes the proof obvious. ■

This result is important because it shows that the implicit scheme is linearly stable:

PROPOSITION 4.1. *The implicit scheme is linearly stable for all* $\delta t > 0$.

For completeness, we include a proof of this proposition in the Appendix.

The preconditioned flux has another interesting property which can be related to the local extremum diminishing property for scalar equations or the total variation diminishing property in the 1-D case. Let $\mathbf{A}^{\text{pos}} = \frac{1}{2}(\mathbf{A} + \mathbf{\Theta})$ and $\mathbf{A}^{\text{neg}} = \frac{1}{2}(\mathbf{A} - \mathbf{\Theta})$. For the unpreconditioned flux, $\mathbf{A}^{\text{pos}} = \mathbf{A}^+$ has only non-negative eigenvalues, and $\mathbf{A}^{\text{neg}} = \mathbf{A}^-$ has only non-positive eigenvalues. This is no longer true for the preconditioned flux, but the following property holds:

PROPERTY 4.2. $\mathbf{SA}^{\text{pos}}$ *is symmetric positive semi-definite and* $\mathbf{SA}^{\text{neg}}$ *is symmetric negative semi-definite.*

4.4. *Application to the Euler Equations*

Symmetrizing the Jacobian matrix is not only useful for showing theoretical results, it also gives a nice formulation of the preconditioned scheme and makes the computation of the eigen-decomposition easier. As an illustration, we give the expressions of two well-known preconditioners, namely Turkel's diagonal preconditioner and the van Leer–Lee–Roe (VLLR) preconditioner.

For the Euler equations, a possible symmetrizing matrix is given by

$$\mathbf{R} = \begin{pmatrix} \chi + \frac{\kappa}{2}|\mathbf{u}|^2 & -\kappa\mathbf{u}^T & \kappa \\ -c\mathbf{u} & c\mathbf{I} & \mathbf{0} \\ -\kappa(H - |\mathbf{u}|^2) & -\kappa\mathbf{u}^T & \kappa \end{pmatrix}, \qquad \mathbf{R}^{-1} = \frac{1}{c^2}\begin{pmatrix} 1 & \mathbf{0}^T & -1 \\ \mathbf{u} & c\mathbf{I} & -\mathbf{u} \\ H & c\mathbf{u}^T & -\frac{1}{2}|\mathbf{u}|^2 \end{pmatrix}.$$

We have denoted by $\mathbf{I}$ and $\mathbf{0}$ the identity matrix and the null vector of $\mathbb{R}^d$. The symmetrized Jacobian $\tilde{\mathbf{A}}_\mathbf{n} = \mathbf{R}\mathbf{A}\mathbf{R}^{-1}$ takes the form

$$\tilde{\mathbf{A}}_\mathbf{n} = \begin{pmatrix} \mathbf{u}\cdot\mathbf{n} & c\mathbf{n}^T & 0 \\ c\mathbf{n} & (\mathbf{u}\cdot\mathbf{n})\mathbf{I} & \mathbf{0} \\ 0 & \mathbf{0}^T & \mathbf{u}\cdot\mathbf{n} \end{pmatrix}.$$

We can see that the last variable (related to the entropy) is totally uncoupled (at least linearly) from the others and will not be affected by preconditioning.

With this change of variables, we can define the preconditioner $\mathbf{P}$ as $\mathbf{R}^{-1}\tilde{\mathbf{P}}\mathbf{R}$.

4.4.1. Computation of the viscosity matrix. The viscosity matrix $\mathbf{P}^{-1}|\mathbf{P}\mathbf{A}|$ can still be written as a sum of rank-one matrices (cf. Subsection 3.2),

$$\mathbf{P}^{-1}|\mathbf{P}\mathbf{A}| = \sum_i |\check{\lambda}_i|\check{\mathbf{r}}_i \otimes \check{\mathbf{l}}_i. \tag{11}$$

However, this decomposition is no longer an eigen-decomposition. Although $\mathbf{P}\mathbf{A}$ can be diagonalized directly, it is often easier to work with the symmetric form, $\mathbf{Q}\tilde{\mathbf{A}}\mathbf{Q}^T$. The eigenvalues of this matrix give the $\check{\lambda}_i$ of the decomposition (11). Let $\mathbf{v}_i$ denote the corresponding eigenvectors. Since

$$\mathbf{Q}\tilde{\mathbf{A}}\mathbf{Q}^T = \sum_i \check{\lambda}_i \mathbf{v}_i \otimes \mathbf{v}_i,$$

we have

$$\tilde{\mathbf{A}} = \sum_i \check{\lambda}_i (\mathbf{Q}^{-1}\mathbf{v}_i) \otimes (\mathbf{v}_i\mathbf{Q}^{-T}),$$

and

$$\mathbf{A} = \sum_i \check{\lambda}_i (\mathbf{R}^{-1}\mathbf{Q}^{-1}\mathbf{v}_i) \otimes (\mathbf{v}_i\mathbf{Q}^{-T}\mathbf{R}).$$

Therefore

$$\check{\mathbf{r}}_i = \mathbf{R}^{-1}\mathbf{Q}^{-1}\mathbf{v}_i, \qquad \check{\mathbf{l}}_i = \mathbf{v}_i\mathbf{Q}^{-T}\mathbf{R}.$$

Since the preconditioner does not change the signs of the $\check{\lambda}_i$, an efficient algorithm like Algorithm 1 (see Definition 3.1) can still be used.

4.4.2. Turkel's preconditioner. Turkel's diagonal preconditioner is given in symmetric form as

$$\tilde{\mathbf{P}} = \mathrm{diag}(\beta^2, \mathbf{I}, 1), \tag{12}$$

where β is of the order of the Mach number. Obviously, this preconditioner can be expressed under the form $\tilde{\mathbf{P}} = \mathbf{Q}^T\mathbf{Q}$, with $\mathbf{Q} = \mathrm{diag}(\beta, \mathbf{I}, 1)$.

The parameter β can be set to a constant reference value of the Mach number. In our case however, it is crucial to use a local value to accommodate the large variations of the Mach number,

$$\beta = \frac{|\tilde{\mathbf{u}}|}{c},$$

where $\tilde{\mathbf{u}}$ and c are the interface average values (see Subsection 3.2). Other choices for β have been investigated recently by Darmofal and Siu [7], to enhance the stability of the scheme near stagnation points, where the local Mach number can reach 0.

We now give the equivalent of Algorithm 1 for Turkel's preconditioner. In the subsonic case, $|\tilde{u}_n| < c$, we set

$$\nu = (1-\beta^2)\tilde{u}_n/2, \qquad \gamma = \sqrt{\nu^2 + \beta^2 c^2}, \qquad \alpha^{\pm} = \gamma \pm \nu.$$

DEFINITION 4.1 (Algorithm 2). .

- If $|\tilde{u}_n| > c$, the scheme is totally upwind:
  —if $\tilde{u}_n > 0$, $\Phi = F(U_L)$,
  —if $\tilde{u}_n < 0$, $\Phi = F(U_R)$.
- In the subsonic case $|\tilde{u}_n| \le c$:
  —if $\tilde{u}_n > 0$, $\Phi = F(U_L) + (\tilde{u}_n - \alpha^+)(\Delta U)^-$
  —if $\tilde{u}_n \le 0$, $\Phi = F(U_R) - (\tilde{u}_n + \alpha^-)(\Delta U)^+$,

with the following definition for $(\Delta U)^{\pm}$,

$$(\Delta U)^{\pm} = \frac{[\![p]\!] \pm \tilde{\rho}\alpha^{\pm}[\![u_n]\!]}{2\alpha^{\pm}\gamma} \begin{pmatrix} 1 \\ \tilde{\mathbf{u}} \pm \alpha^{\pm}\mathbf{n} \\ \tilde{H} \pm \tilde{u}_n\alpha^{\pm} \end{pmatrix}.$$

Note that when $\beta = 1$, we have $\gamma = \alpha^+ = \alpha^- = c$, and the original Roe scheme (Algorithm 1) is recovered.

4.4.3. The VLLR Preconditioner. The van Leer–Lee–Roe preconditioner for 2-D subsonic flow can be expressed as $\tilde{\mathbf{P}} = \mathbf{Q}^T\mathbf{Q}$, where $\mathbf{Q}$ is the product of an upper triangular and a rotation matrix,

$$\mathbf{Q} = \begin{pmatrix} M & -1 & 0 & 0 \\ 0 & 1 & 0 & 0 \\ 0 & 0 & \sqrt{1-M^2} & 0 \\ 0 & 0 & 0 & 1 \end{pmatrix} \cdot \begin{pmatrix} 1 & 0 & 0 & 0 \\ 0 & u_x/q & u_y/q & 0 \\ 0 & -u_y/q & u_x/q & 0 \\ 0 & 0 & 0 & 1 \end{pmatrix}.$$

In the original VLLR preconditioner, the second coefficient on the diagonal of $\mathbf{Q}$ is actually different: the difference is irrelevant in our case since it does not change the artificial

viscosity $\mathbf{P}^{-1}|\mathbf{PA}|$. In 3-D, the corresponding rotation matrix is not uniquely defined, and a choice has to be made.

The preconditioned Jacobian takes the form

$$\mathbf{Q}\tilde{\mathbf{A}}\mathbf{Q}^T = \begin{pmatrix} u_n(M^2-1) & 0 & u_\tau\sqrt{1-M^2} & 0 \\ 0 & u_n & 0 & 0 \\ u_\tau\sqrt{1-M^2} & 0 & u_n(1-M^2) & 0 \\ 0 & 0 & 0 & u_n \end{pmatrix},$$

with $u_n = u_x n_x + u_y n_y$ and $u_\tau = -u_x n_y + u_y n_x$. This matrix has another uncoupled variable, which is related to the transport of the total enthalpy along streamlines at steady state (see [30]).

We now give the equivalent of Algorithm 1 for this preconditioner. In the subsonic case, $|\tilde{u}_n| < c$, we set

$$\nu = \tilde{u}_n\sqrt{1-M^2}, \qquad \gamma = \sqrt{\nu^2 + u_\tau^2}.$$

We denote by $\tilde{\mathbf{u}}^T = (-u_y, u_x)$ the vector obtained by a $\pi/2$ rotation of $\mathbf{u}$. We then introduce $\theta = \mathrm{Atan}(u_\tau/\nu)/2$. Then the preconditioned scheme is given by:

DEFINITION 4.2 (Algorithm 3). .

- If $|\tilde{u}_n| > c$, the scheme is totally upwind:
  —if $\tilde{u}_n > 0$, $\Phi = F(U_L)$,
  —if $\tilde{u}_n < 0$, $\Phi = F(U_R)$.
- In the subsonic case $|\tilde{u}_n| \le c$:
  —if $\tilde{u}_n > 0$, $\Phi = F(U_L) - \gamma\sqrt{1-M^2}(\Delta U)^-$
  —if $\tilde{u}_n \le 0$, $\Phi = F(U_R) - \gamma\sqrt{1-M^2}(\Delta U)^+$,

with the following definitions for $(\Delta U)^\pm$,

$$(\Delta U)^+ = \frac{1}{|\tilde{\mathbf{u}}|^2}\left(\cos\theta[\![p]\!] + \sin\theta\frac{\tilde{\mathbf{u}}^T}{\sqrt{1-M^2}}[\![\rho\mathbf{u}]\!]\right)\begin{pmatrix} \cos\theta \\ \cos\theta\,\tilde{\mathbf{u}} + \sin\theta\frac{\tilde{\mathbf{u}}^T}{\sqrt{1-M^2}} \\ \cos\theta\,\tilde{H} \end{pmatrix},$$

and

$$(\Delta U)^- = \frac{1}{|\tilde{\mathbf{u}}|^2}\left(\sin\theta[\![p]\!] - \cos\theta\frac{\tilde{\mathbf{u}}^T}{\sqrt{1-M^2}}[\![\rho\mathbf{u}]\!]\right)\begin{pmatrix} \sin\theta \\ \sin\theta\,\tilde{\mathbf{u}} - \cos\theta\frac{\tilde{\mathbf{u}}^T}{\sqrt{1-M^2}} \\ \sin\theta\,\tilde{H} \end{pmatrix}.$$

Our experience [4] shows that the numerical results for the two preconditioners are quite similar, although the VLLR preconditioner gives a better prediction of the total enthalpy. On the other hand, Turkel's diagonal preconditioner is easier to implement and has a natural 3-D extension. In the present work, we have only used Turkel's preconditioner.

5. NUMERICAL RESULTS

In this section, we show some numerical results obtained with the time-consistent Roe–Turkel scheme. In all cases, a linearized implicit time-stepping has been used. We first

TABLE I
Initial Data for the Subsonic Acoustic Wave

	At point $(\frac{1}{2}, \frac{1}{2})$	Elsewhere
ρ	1.1	1.
u	0.1	
v	0.01	

compute the evolution of a point-wise perturbation in a uniform subsonic flow. The aim of this test case is to show the effect of preconditioning the numerical flux. Since the properties of the fluid are not important in this test case, we use a simpler barotropic pressure law.

We then turn to the two-phase flow simulations with the homogeneous equilibrium model. We perform a steady-state and an unsteady computation in a "bump channel" geometry.

5.1. *Acoustic Wave*

The first example is the computation of a circular acoustic wave created by a pointwise perturbation in a uniform flow. For this test case, an isentropic model suffices,

$$\partial_t \rho + \operatorname{div}(\rho \mathbf{u}) = 0$$
$$\partial_t \rho \mathbf{u} + \operatorname{div}(\rho \mathbf{u} \otimes \mathbf{u}) + \nabla p(\rho) = 0.$$

We take $p = \frac{1}{2}\rho^2$, so that the resulting system is formally equivalent to the Saint–Venant equations of shallow water.

The initial data for this test case are a constant subsonic state ($M = 0.1$) with a point-wise disturbance (see Table I). The exact solution is a circular acoustic wave expanding in time and slowly advected with the flow. This simple test case aims at revealing the grid sensitivity of the scheme.

We perform five implicit time steps with $\delta t/\delta x = 1$. A regular 60×60 mesh is used. The numerical results for Roe's scheme and Turkel's preconditioner are shown in Figs. 2, 3.

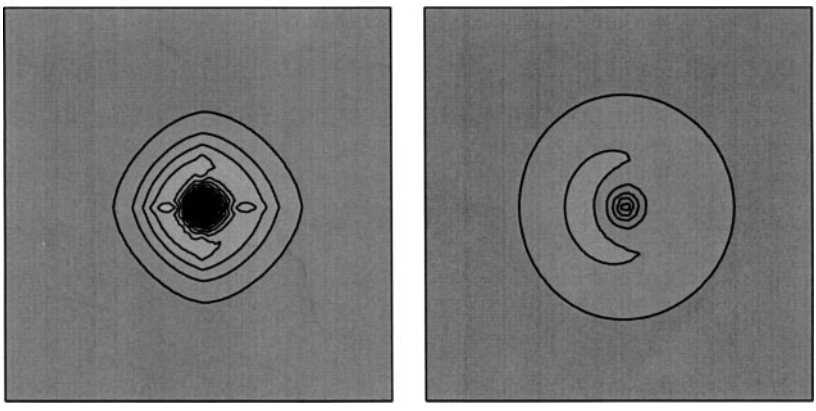

FIG. 2. Acoustic wave test case: density field. Notice the regularity of the wave front computed by the Roe–Turkel scheme. The speed of propagation of the wave front is not affected by preconditioning, but the amplitude of the variations diminishes.

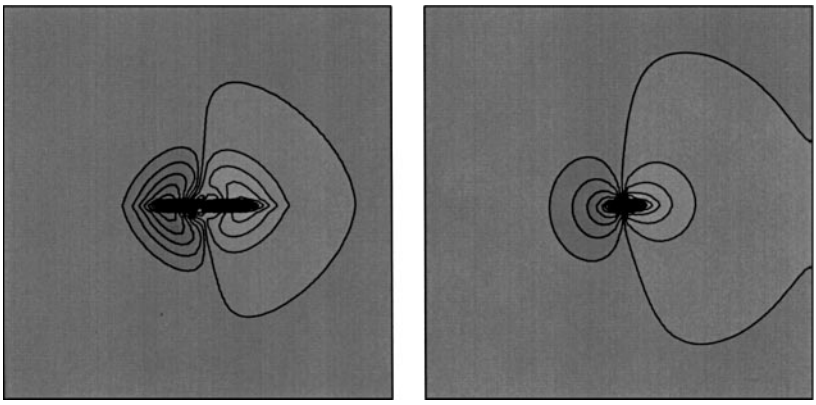

FIG. 3. Acoustic wave test case: Mach number field. Notice the discontinuity aligned with the x grid line with Roe's scheme. The Roe–Turkel solution is smoother.

For each scheme, we present the density field and the Mach number $M = |u|/c$. The solution computed by the Roe scheme presents a squarish wave front with discontinuities aligned with the grid lines. The Mach number field shows an important discontinuity which is aligned with the x grid line originating from the initial perturbation.

The solution given by the preconditioned scheme is smoother and less sensitive to the mesh geometry. The extension of the wave front is correct, which shows that the time-accuracy is not destroyed by preconditioning. The amplitude of the density variations is larger for the Roe than for the Roe–Turkel scheme, which shows that more numerical diffusion is added on the first equation. On the Mach number field however, the numerical diffusion of the preconditioned scheme is smaller. Above all, the numerical diffusion is almost isotropic, which is not the case for the unpreconditioned scheme.

5.2. *Two-Phase Flow in a Channel with Bump*

This section deals with the simulation of the homogeneous equilibrium model (1) introduced in the first section. We consider a channel with a 20% sinusoidal bump (Fig. 4). The boundary conditions are specified in Table II. At the inflow, the fluid is liquid but very close to the saturation. As the pressure drops with the restriction of the section, a small concentration of vapor appears. The Mach number changes dramatically after the transition. In the first test case, the inlet velocity is such that the flow remains completely subsonic, although with important compressibility effects. In the second test case, however, the Mach number reaches one at the throat and a shock appears behind the bump.

The existence of shocks in flows with area restriction is particularly important for dimensioning pipes, since they determine the maximum flow rate that can be reached. Although

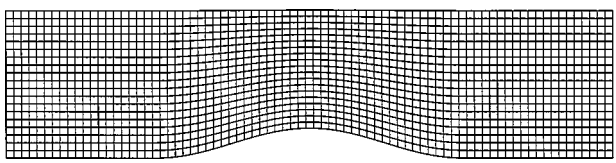

FIG. 4. Channel with bump: 20×80 structured mesh.

TABLE II
Boundary Conditions for the Two-Phase Bump Channel Flow

Inflow			Outflow
h	1154.2 kJ/kg		
u	10. m · s^{-1}	p	50. 10^5 Pa
v	0. m · s^{-1}		

stationary shocks are rarely found in common liquid flows, they easily occur after a two-phase transition. This problem has been intensely studied over the years, principally with one-dimensional analyses (see, e.g., [24]. It is our hope that multidimensional simulations will provide useful additional information for the design of valves and pipes subject to phase transition.

5.3. *Subsonic Solution*

This computation is performed with a constant time step of 10^{-1}. Convergence is reached in less than 40 time steps (see Fig. 7). To monitor the convergence, we study the decrease of the norm of the residual, i.e., the right hand side in Eq. (10).

The pressure profile is displayed in Fig. 5. As expected, no discontinuity can be detected across the phase transition lines. However, the influence of the vapor is clearly visible on the Mach number profile (Fig. 6, right), which shows sharp discontinuities. For both profiles, the symmetry is quite satisfactory.

We also display the total enthalpy along the walls (Fig. 7) which should be constant in this irrotational flow, according to Bernoulli's theorem. The observed variation is typical of a first order scheme. We underline the fact that no jump in the enthalpy can be observed across the transition lines.

5.4. *Transonic Flow*

In this test case, the inlet velocity is higher (see Table III). The flow reaches Mach 1 at the throat and a stationary shock forms behind the bump. The fluid then goes back to the liquid state and the Mach number drops back to a small value.

For this test case, one must use smaller time steps because of the presence of the stationary shock. The time-step is first set to $5 \cdot 10^{-2}$ during 6 iterations, then reset to $5 \cdot 10^{-3}$ as the shock starts forming. After 100 iterations, the residual has lost 4 orders of magnitude. The solution is displayed in Fig. 8 (pressure field) and Fig. 9 (Mach number field). Due to the large variations of the Mach number across the phase transition line, the shock is hardly visible. It is more easily seen on the pressure field. A better resolution of the shock would be obtained with a finer mesh or a higher order discretization.

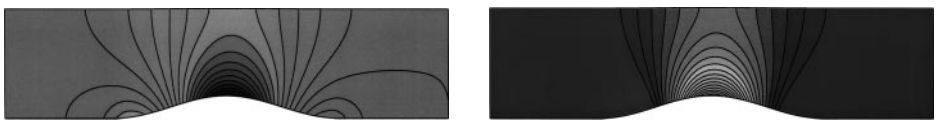

FIG. 5. Channel with bump. Left, pressure (min $= 49.54 \cdot 10^5$ Pa, max $= 50.11 \cdot 10^5$ Pa, 20 isolines). Right, vapor concentration (min $= 0$, max $= 1.66 \cdot 10^{-3}$, 20 isolines).

TABLE III
Boundary Conditions for the Two-Phase Transonic Flow

Inflow			Outflow
h	1154. kJ/kg		
u	24. $m \cdot s^{-1}$	p	50. 10^5 Pa
v	0. $m \cdot s^{-1}$		

FIG. 6. Channel with bump. Logarithm of the Mach number (min $= 7.668 \cdot 10^{-3}$, max $= 0.4136$, 80 isolines in logarithmic scale). Note the sharp discontinuity along the phase transition line.

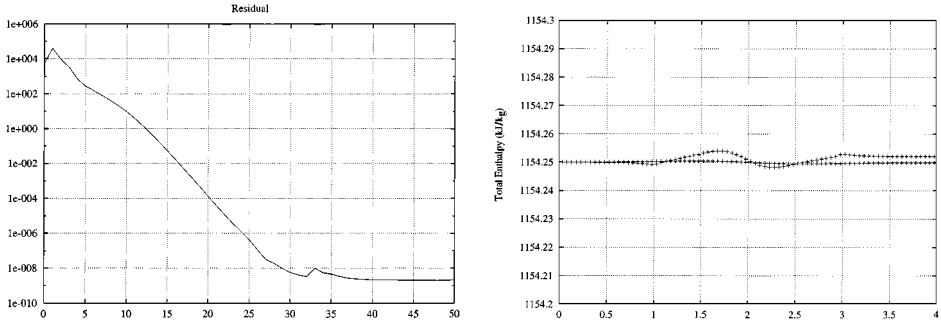

FIG. 7. Channel with bump. Left, history of the residual in L^2 norm. Right, total enthalpy on the walls.

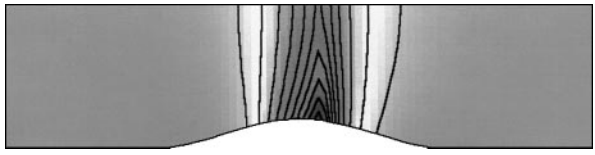

FIG. 8. Transonic flow in a channel with bump: pressure field (min $= 39.908 \cdot 10^5$ Pa, max $= 50.948 \cdot 10^5$ Pa, 10 isolines).

FIG. 9. Transonic flow in a channel with bump: Mach number field (min $= 1.518 \cdot 10^{-2}$, max $= 1.0903$, 10 isolines).

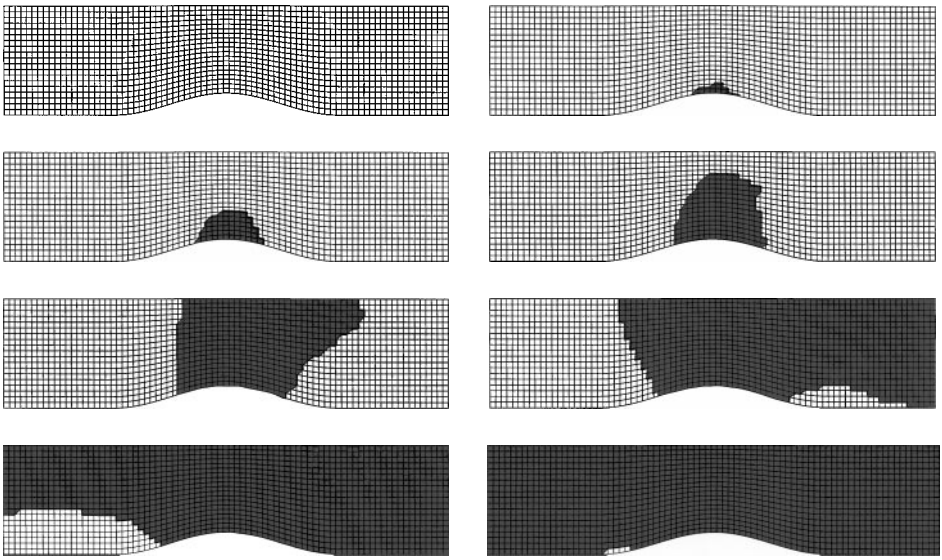

FIG. 10. Loss of pressure simulation. Cells occupied by the liquid (white) or the two-phase mixture (black). From left to right and top to bottom: time steps 5, 10, 15, 20, 25, 30, and 35 10^{-3} s.

5.5. *Unsteady Flow*

The time-consistent preconditioned solver is particularly intersting for the simulation of unsteady flows. To illustrate this feature, we compute a flow with a varying outflow boundary condition. The imposed pressure at outflow drops linearly from $p = 50.4 \cdot 10^5$ Pa at $t = 0$ to $p = 49.4 \cdot 10^5$ pa at $t = 0.5$ s. The inlet enthalpy and velocity are kept constant. The time-step is still $\delta t = 5 \cdot 10^{-3}$ s. We observe the evolution in time of the transition between the liquid and the two-phase mixture (Fig. 10). We can see the growth of the two-phase patch which finally occupies the whole channel.

6. CONCLUSION

Two-phase flows are characterized by large variations of the Mach number, due to the different compressibility of the liquid and the two-phase mixture. We have shown that a preconditioned finite volume scheme based on Roe's numerical flux is able to simulate such flows, both for steady-state and unsteady applications. From the theoretical point of view, the robustness of the solver can be linked to a generalization of the local extremum diminishing property which is satisfied by the class of preconditioned upwind solvers.

The numerical results obtained with this method for steady-state and unsteady problems seem satisfactory, although we still lack analytical or numerical results to validate them.

One could improve the efficiency by turning to a partially implicit scheme, in order to reduce the size of the Jacobian matrix. The spatial accuracy should be improved by introducing either a MUSCL-type reconstruction or a discontinuous-Galerkin method. For unsteady problems, the use of a high order time-discretization would also be necessary. This question is currently under examination; our concern is to keep the method efficient, which is not so obvious for a fluid with a non-linear equation of state. In a recent study [6], we have shown that spurious acoustic waves may occur in the vicinity of contact discontinuities and

perturb transient simulations. Note that this phenomenon is not specific to our solver but rather comes from the conservation form of the equations.

Finally, one would like to extend the numerical method to more general two-phase flow models including kinematic and/or thermodynamic non-equilibrium effects. Whereas relaxing the thermodynamic equilibrium should not be a serious problem, a number of issues must be addressed to simulate kinematic non-equilibrium models. First, one has to construct an upwind compressible solver for the system of equations considered. This issue is already quite a difficult one and is still an active area of research. Next, one should define a preconditioner for the system. Here the major difficulty is to define the typical order of magnitude of the pressure fluctuations. In a homogeneous low speed flow, they are of the order of ρu^2, where u is the reference velocity of the fluid. With a model including two velocities and one pressure, the picture is not so clear. Finally, our numerical method relies on a coupled fully implicit formulation, which will be more difficult to handle in a model with a large number of unknowns.

A. APPENDIX

Linear Stability of Implicit Finite Volume Schemes

In this appendix, we prove the linear stability of the implicit scheme, in the case of a symmetric system with constant coefficients,

$$\partial_t U + \sum \mathbf{A}^\alpha \partial_\alpha U = 0.$$

The matices $\mathbf{A}^\alpha, \alpha = 1, \dots d$, are constant symmetric matrices. In the linear case, the upwind flux can be written in the form

$$\Phi(\mathbf{n}, U_L, U_R) = \frac{1}{2}\mathbf{A}_\mathbf{n}(U_L + U_R) - \frac{1}{2}\mathbf{\Theta}_\mathbf{n}(U_R - U_L). \tag{13}$$

The proof applies to any numerical flux with a symmetric positive semi-definite viscosity matrix $\mathbf{\Theta}$ such that $\mathbf{\Theta}_\mathbf{n} = \mathbf{\Theta}_{-\mathbf{n}}$. In particular, the preconditioned flux belongs to this category.

For simplicity, we write $\Phi_{KJ} = \Phi(U_K, U_J)$, $\mathbf{A}_{KJ} = \mathbf{A}_{\mathbf{n}_{KJ}}$, and $\mathbf{\Theta}_{KJ} = \mathbf{\Theta}_{\mathbf{n}_{KJ}}$. We denote by $\mathcal{U} = (U_K)_{K\in\mathcal{T}_h}$ the vector whose components are the discrete values of U in each cell. The notation $\mathcal{M}$ will refer to the matrix of the discrete flux operator. Specifically, the component of the vector $\mathcal{M}U$ corresponding to the cell K reads

$$(\mathcal{M}U)_K = \frac{1}{2|K|}\sum_{J\in\mathcal{N}(K)} |\partial K \cap \partial J|[\mathbf{A}_{KJ}(U_K + U_J) - \mathbf{\Theta}_{KJ}(U_J - U_K)]. \tag{14}$$

To simplify the analysis, we consider the case of periodic boundary conditions.

With the preceding notations, the implicit finite volume scheme takes the compact form,

$$(Id + \delta t\mathcal{M})\mathcal{U}^{n+1} = \mathcal{U}^n.$$

We finally introduce a discrete L^2 scalar product,

$$(\mathcal{U}, \mathcal{V}) = \sum_K |K| U_K \cdot V_K.$$

To prove the stability of the implicit scheme, we need to show that:

LEMMA A.1. *For all vectors $\mathcal{U}$,*

$$(\mathcal{M}U, \mathcal{U}) \geq 0.$$

Proof. We first compute $(\mathcal{M}U, \mathcal{U})$ by taking the scalar product of each equality (14) with $|K|\mathcal{U}_K$, and summing over all cells,

$$(\mathcal{M}U, \mathcal{U}) = \sum_K \sum_{J \in \mathcal{N}(K)} |\partial K \cap \partial J| \Phi_{KJ} \cdot U_K.$$

In this sum, we split the centered and the upwind part. Let

$$E_1 = \frac{1}{2} \sum_K \sum_{J \in \mathcal{N}(K)} |\partial K \cap \partial J| \mathbf{A}_{KJ}(U_K + U_J) \cdot U_K$$

and

$$E_2 = \frac{1}{2} \sum_K \sum_{J \in \mathcal{N}(K)} |\partial K \cap \partial J| \mathbf{\Theta}_{KJ}(U_K - U_J) \cdot U_K.$$

We note that the term

$$\sum_{J \in \mathcal{N}(K)} |\partial K \cap \partial J| \mathbf{A}_{KJ} = \int_{\partial K} \mathbf{A} \cdot \mathbf{n}\, ds$$

vanishes in the case of constant coefficients.

We can now rewrite E_1 as a sum over all edges of the triangulation,

$$E_1 = \frac{1}{2} \sum_{\partial K \cap \partial J} |\partial K \cap \partial J| [\mathbf{A}_{KJ} U_J \cdot U_K + \mathbf{A}_{JK} U_K \cdot U_J].$$

Since $\mathbf{A}_\mathbf{n}$ is symmetric and $\mathbf{A}_{KJ} = -\mathbf{A}_{JK}$, we have $E_1 = 0$.

We perform a similar manipulation on the second term. We first rewrite E_2 as a sum over all the interfaces of the triangulation,

$$E_2 = \frac{1}{2} \sum_{\partial K \cap \partial J} |\partial K \cap \partial J| [\mathbf{\Theta}_{KJ}(U_K - U_J) \cdot U_K + \mathbf{\Theta}_{JK}(U_J - U_K) \cdot U_J]. \tag{15}$$

Now since $\mathbf{\Theta}$ is symmetric and $\mathbf{\Theta}_{KJ} = \mathbf{\Theta}_{JK}$, we can rewrite E_2 as

$$\begin{aligned} E_2 &= \frac{1}{2} \sum_{\partial K \cap \partial J} |\partial K \cap \partial J| [\mathbf{\Theta} U_K \cdot U_K - 2\mathbf{\Theta} U_K \cdot U_J + \mathbf{\Theta} U_J \cdot U_J] \\ &= \frac{1}{2} \sum_{\partial K \cap \partial J} |\partial K \cap \partial J| \mathbf{\Theta}_{KJ}(U_K - U_J) \cdot (U_K - U_J). \end{aligned} \tag{16}$$

Thus, $(\mathcal{M}\mathcal{U}, \mathcal{U})$ is a sum of non-negative terms, and the proof is complete. ∎

The stability of the implicit scheme follows from this inequality.

PROPOSITION A.1. *The implicit scheme is linearly stable for all* $\delta t > 0$.

Proof. We simply remark that

$$(\mathcal{U}^{n+1}, \mathcal{U}^{n+1}) = (\mathcal{U}^n, \mathcal{U}^{n+1}) - \delta t (\mathcal{M}\mathcal{U}^{n+1}, \mathcal{U}^{n+1}) \leq (\mathcal{U}^n, \mathcal{U}^{n+1}).$$

Hence $(\mathcal{U}^{n+1}, \mathcal{U}^{n+1}) \leq (\mathcal{U}^n, \mathcal{U}^n)$ by the Schwarz inequality. ∎

REFERENCES

1. H. Bijl and P. Wesseling, A unified method for computing incompressible and compressible flows in boundary-fitted coordinates, *J. Comput. Phys.* 153 (1998).
2. M. Breuer and D. Hänel, A dual time-stepping method for 3-D, viscous, incompressible vortex flow, *Comput. & Fluids* **22**, 467 (1993).
3. Y. H. Choi and C. L. Merkle, The application of preconditioning in viscous flows, *J. Comput. Phys.* **105**, 207 (1993).
4. S. Clerc, *Etude de schémas décentrés implicites pour le calcul numérique en mécanique des fluides—Résolution par décomposition de domaine*, Tech. Rep. CEA-R-5797, Commissariat à l'Energie Atomique, 1998 (unpublished).
5. S. Clerc, On the preconditioning of finite volume schemes, in *Proceedings of the 7th Int. Conf. on Hyperbolic Problems, Zürich, 1998.*
6. S. Clerc, Accurate computation of contact discontinuities in flows with general equations of state, *Comput. Methods Appl. Mech. Eng.* **178**, 245 (1999).
7. D. L. Darmofal and K. Siu, A robust multigrid algorithm for the Euler equations with local preconditioning and semi-coarsening, *J. Comput. Phys.* **151**, 728 (1999).
8. A. T. Fedorchenko, A model of unsteady subsonic flow with acoustic excluded, *J. Fluid Mech.* 135 (1997).
9. M. Grandotto and P. Obry, Calcul des écoulements diphasiques dans les échangeurs par une méthode aux éléments finis, *Rev. Europ. Eléments Finis* **5**(1), (1996).
10. H. Guillard and C.Viozat, On the behaviour of upwind schemes in the low Mach number limit, *Comput. & Fluids* 63 (1999).
11. A. Jameson, Analysis and design of numerical schemes for gas dynamics. I. Artificial diffusion, uwpind biasing, limiters and their efficiency on accuracy and multigrid convergence, *Int. J. Comput. Fluid Dyn.* **5**, 171 (1995).
12. R. Klein, Semi-implicit extension of a Godunov-type scheme based on low Mach number asymptotics. I. One-dimensional flow, *J. Comput. Phys.* **121**, 213 (1995).
13. S. Kotake and I. I. Glass, Flows with nucleation and condensation, *Prog. Aeorospace Sci.* **19**, 129 (1981).
14. M.-S. Liou, A sequel to AUSM: AUSM+, *J. Comput. Phys.* **129**, 364 (1996).
15. A. Majda, *Compressible Fluid Flow and Systems of Conservation Laws in Several Space Variables* (Springer-Verlag, New York/Berlin, 1994), Chap. 2.
16. R. Menikoff and B. J. Plohr, The Riemann problem for fluid flow of real materials, *Rev. Mod. Phys.* **61**, 75 (1989).
17. L. Mottura, L. Vigevano, and M. Zaccanti, An evaluation of Roe's scheme generalizations for equilibrium real gas flows, *J. Comput. Phys.* **138**, 354 (1997).
18. C.-D. Munz and S. Roller, A low Mach number scheme based on the multiple pressure variables approach, in *Proceedings of the 4th ECCOMAS Conf. on Comput. Fluid Dynamics, Athens* (Wiley, New York, 1998).
19. H. Paillère and J.P. Magnaud, A finite element elliptic flow solver for low Mach number compressible flows, in *10th Int. Conf. on Finite Elements in Fluids, Tucson, 1998.*
20. H. Paillère, S. Clerc, C. Viozat, I. Toumi, and J.-P. Magnaud, Numerical methods for low Mach number thermal-hydraulic flows, in *Proceedings of the 4th ECCOMAS Conf. on Comput. Fluid Dynamics, Athens* (Wiley, New York, 1998).
21. S. Paolucci, *On the Filtering of Sound from the Navier–Stokes Equations*, Tech. Rep. 8257, Sandia National Lab., 1982 (unpublished).
22. T. A. Porsching, A finite difference method for thermally expandable fluid transients, *Nucl. Sci. Eng.* **64**, 177 (1977).
23. P. L. Roe, Approximate Riemann solvers, parameter vectors, and difference schemes, *J. Comput. Phys.* **43**, 357 (1981).
24. V. E. Schrock and C. N. Amos, Two-phase critical flow, in *Two-Phase Flow and Heat Transfer, China US Progress*, edited by Chen and Veziroglu (Hemisphere, Washington, DC, 1984), p. 115.
25. D. Serre, *Systèmes de lois de conservation* (Diderot, Paris, 1996), Vol. I, Chap. 3.

26. H. B. Stewart and B. Wendroff, Two-phase flow: Models and methods, *J. Comput. Phys.* **56**, 363 (1984).
27. I. Toumi, A weak formulation of Roe's approximate Riemann solver, *J. Comput. Phys.* **102**, 360 (1991).
28. E. Turkel, Preconditioned methods for solving the incompressible and low speed compressible equations, *J. Comput. Phys.* **72**, 277 (1987).
29. E. Turkel, Review of preconditioning methods, *Appl. Numer. Math.* **12**, 257 (1993).
30. B. van Leer, W.-T. Lee, and P. L. Roe, *Characteristic Time-Stepping or Local Preconditioning of the Euler Equations*, AIAA paper 1552, 1991.
31. S. Venkateswaran and C. L. Merkle, *Dual Time Stepping and Preconditioning for Unsteady Computations*, AIAA paper 95-0078, 1995.
32. M. Vinokur and J. L. Montagné, Generalized flux-vector splitting and Roe-average for an equilibrium real gas, *J. Comput. Phys.* **89**, 276 (1990).
33. C. Viozat, *Implicit Upwind Schemes for Low Mach Number Compressible Flows*, Tech. Rep. 3084, INRIA, 1997.
34. G. Volpe, Performance of compressible flow codes at low Mach numbers, *AIAA J.* **31**, 49 (1974).